Reusable homogeneous metal- and additive-free photocatalyst for high-performance aerobic oxidation of alcohols to carboxylic acids

Jing-Wang Cui, Shuai Ma, Cai-Hui Rao, Meng-Ze Jia, Xin-Rong Yao, Jie Zhang [*]

MOE Key Laboratory of Cluster Science, Beijing Key Laboratory of Photoelectronic/Electrophotonic Conversion Materials, School of Chemistry and Chemical Engineering, Beijing Institute of Technology, Beijing 102488, PR China

A R T I C L E   I N F O

A B S T R A C T

How to realize the recycling of homogeneous catalysts has been a great challenge for chemists. In this background, a new pyridinium compound was synthesized and applied in selective photocatalytic oxidation. This photocatalytic system is advantageous in accelerating the transformation of alcohols into acids by two consecutive routes, including (1) photocatalytic oxidation of alcohols to aldehydes; (2) photocatalytic oxidation and autoxidation of aldehydes to acids. By activating molecular oxygen into $\bullet O_2^-$ and $^1O_2$, the system displays advantages of high efficiency and simplicity, as well as environment-friendly nature without metals or additives. Attractively, this compound as a homogeneous catalyst can be reused by direct filtration of products profiting from its high performance and stability. The present work develops a new approach to achieve an efficient and recyclable aerobic oxidation of alcohols into acids by using pyridinium-based photocatalysts and provides a valuable insight into the separation and recycling of homogeneous catalysts for economic compatibility and industrial application.

1. Introduction

Direct oxidation of primary alcohols into carboxylic acids has been an essential synthetic process in both academic research and industrial production [1–3]. However, the traditional method for this transformation is carried out generally by using undesirable stoichiometric oxidants, of which the main drawback is to bring about a negative environmental impact through producing harmful byproducts [4]. Recently the dehydrogenative alcohol oxidation system without using harmful oxidants to access carboxylate salts has gained intense attention [5–12], while the need of expensive metals or corrosive bases severely limits its practical application. Hence to accord with the green and sustainable development, it is very necessary to develop new metal- and base-free catalytic strategies for the conversion of alcohols into carboxylic acids.

Homogeneous photocatalysis involving small organic molecules [13–19] has exhibited particular significance in making the best of sustainable solar energy and molecular oxygen (O$_2$) as a green oxidant [20,21], but it has not been well developed in the realm of catalytic transformation of alcohols to carboxylic acids. On the other side, the further development of the homogeneous catalytic system is severely restricted by the main disadvantage in the recycling of catalysts, although it is more superior in catalytic efficiency compared with the heterogeneous system. Currently, the main strategies to separate homogeneous catalysts, including the catalyst extraction and solvent evaporation, are unsatisfactory, mainly for the complexity and inefficiency [22]. On this basis, an opposite perspective about separating the product directly and effectively according to the variation in solubility between the homogeneous catalyst and product was put forward to solve these aforementioned problems. Just as Madsen and Li independently demonstrated that the desired product potassium carboxylate was precipitated from toluene, meanwhile the filtrate containing catalysts could be reused [23,24]. But the use of stoichiometric corrosive base and subsequent acidification operation in such a system is unable to satisfy the demand for the sustainable development and practical production.

The pyridinium derivatives, typically viologen compounds, have been the focus of chemists relying on their excellent photoelectrochemical properties and the character of easy modification [25–31]. Given that the pyridinium can activate molecular oxygen by electron transfer or energy transfer with the simultaneous generation of $\bullet O_2^-$ or $^1O_2$, our group first use the pyridinium salt as small molecule

photocatalysts to achieve high-performance oxidation of alcohols to aldehydes or ketones without the aid of any metals or additives [32]. During this process, the generation of a small amount of carboxylic acids has been observed during the oxidation of primary alcohols. It is highly desirable to clarify the formation mechanism of carboxylic acids and further explore a possibility of completing the high-performance oxidation of alcohols into carboxylic acids by taking full advantage of no additives, low catalyst loading and high stability of the pyridinium derivative as a green photocatalyst.

Herein, by combining photocatalytic oxidation and autoxidation of aldehydes to acids, we have developed a new protocol for transforming various alcohols into the corresponding acids directly in a green, convenient, and economical way by only using air oxygen as an oxidant and the pyridinium molecule as a photocatalyst, namely **TPT-COOCH₃·Br** (1,1′,1″-tri(dimethyl-3,5-dicarboxylatobenzyl)-4,4′,4″-(1,3,5-triazine-2,4,6-triyl)tripyridinium bromide) (Scheme 1). Besides the efficient, stable, metal- and additive-free characters, the recycling of the homogeneous catalyst can be achieved by filtering out the precipitation of the product in case that the amount of irradiation time and substrate increase simultaneously, promising to realize its application in the industrial production by means of the direct separation of the carboxylic acid product from the homogeneous environment.

2. Experimental section

2.1. Preparation of TPT-COOCH₃·Br

Dimethyl 5-(bromomethyl)isophthalate (10.34 g, 36 mmol) was added into a stirred solution of 2,4,6-tri(4-pyridyl)-1,3,5-triazine (**TPT**) (1.87 g, 6 mmol) in 200 mL *N,N*-dimethylformamide (DMF), and then the reaction temperature remained at 110 °C for 12 h. After the reaction was completed, the resulting precipitate was isolated by hot filtration, washed with DMF three times, and dried in a vacuum to give **TPT-COOCH₃·Br** as a yellow powder (5.00 g, yield 71%). ^{1}H NMR (400 MHz, DMSO-d_6): δ 9.70 (6H, d, J = 4.0 Hz), 9.52 (6H, d, J = 4.0 Hz), 8.58 (6H, s), 8.53 (3H, s), 6.21 (6H, s), 3.93 (18H, s).

2.2. Characterization methods

Photocatalytic reactions were carried out by using multichannel photochemical reaction systems (PerfectLight PCX50C for the photoreaction under 365 nm LED light, SSSTECH-LAL1CV1.0 for the photoreactions under 395 nm and white LED light). Infrared (IR) spectra were measured in the range of 4000–400 cm^{-1} on a Nicolet iS10 FT-IR spectrometer with samples prepared as KBr pellets. Elemental analyses (EA) of C, H, and N were investigated on a Vario EL III CHNOS elemental analyzer. Energy-dispersive X-ray spectroscopy (EDS) measurements were performed on a JSM-6700F scanning electron microscope. Powder

X-ray diffraction (PXRD) patterns were collected on a Bruker D8 Advance X-ray diffractometer with Cu Kα radiation (λ = 1.5406 Å). The UV-Vis absorption properties in solid-state and in solution were both characterized by a PE Lambda 900 spectrometer. Thermogravimetric analyses (TGA) were obtained on a Mettler Toledo TGA/DSC 1/1100 analyzer under air atmosphere with a heating rate of 20 °C min^{-1} from 30 to 1000 °C. ^{1}H NMR spectra were measured on a Bruker AV-400 NMR spectrometer by dissolving samples in a deuterated reagent. X-ray photoelectron spectroscopy (XPS) studies were conducted with a PHI 5000 Versaprobe III X-ray photoelectron spectrometer using Al Kα radiation (X-ray beam spot 200 μm). The XPS fitting was calculated by MultiPak-9.8 software. Electron spin resonance (ESR) measurements were recorded using a JES-FA200 ESR spectrometer. Gas chromatography (GC) analyses were performed on Shimadzu GC-2014 C with the FID detector equipped with an Rtx-5 capillary column.

2.3. Photocatalytic oxidation reaction

As an aprotic solvent, acetonitrile was used as the reaction medium in this photocatalysis. Typically, a clear solution of substrate (0.1 mmol), photocatalyst (1.0 μmol), and acetonitrile (5.0 mL) was added into the special reaction vessel containing a magnetic stir bar. The reaction mixture was stirred open to air through a stainless steel needle for 30 min under room temperature, then irradiated by UV light source. After ending the reaction, the product was confirmed by comparing the GC retention time with that of a pure sample obtained from commercial sources. The conversion (Con.) and selectivity (Sel.) were measured by GC. The turnover frequency (TOF) is expressed as follows:

$$TOF\ (h^{-1}) = (Con. \times n_p)/(n_c \times h)$$

where n_p is the number of moles of the substrate, n_c is the number of moles of the photocatalyst, h is the reaction time.

3. Results and discussion

3.1. Characterization of TPT-COOCH₃·Br

The pyridinium salt **TPT-COOCH₃·Br** was synthesized through a one-step nucleophilic substitution of 2,4,6-tri(4-pyridyl)-1,3,5-triazine (**TPT**) with dimethyl 5-(bromomethyl)isophthalate. Infrared (IR) spectra clearly confirm the occurrence of *N*-alkylation on 4-pyridyl terminal group of **TPT** molecule, as well as the introduction of ester group, as evidenced by the characteristic C=N aromatic stretches of the pyridinium moiety at 1639 cm^{-1}, and the ester group's C=O stretching vibration at 1726 cm^{-1} (details in Fig. S1). ^{1}H NMR spectroscopy reveals that the signals of the pyridinium ring protons appearat 9.70 and 9.52 ppm, while the signal of the ester group at 3.93 ppm (details in
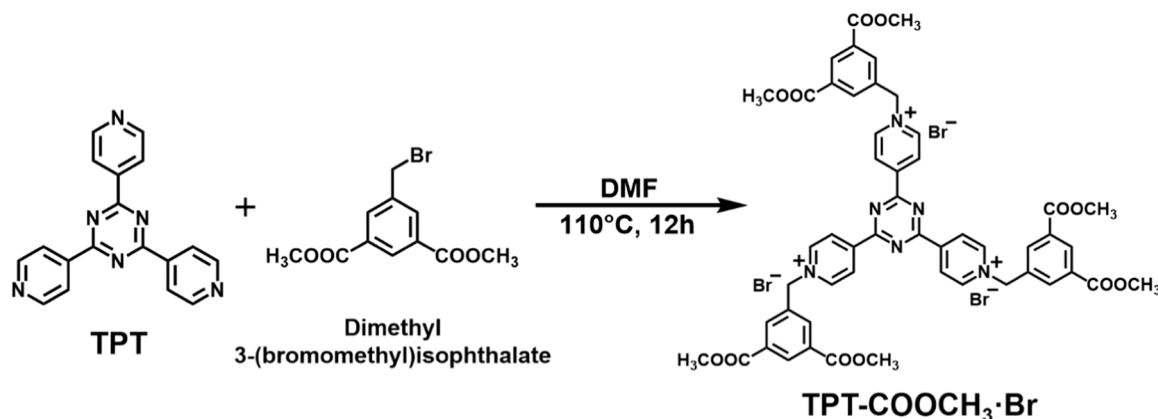
Scheme 1. Synthetic route of TPT-COOCH₃·Br.

Fig. S2). The detailed morphology of the as-synthesized sample is confirmed by the scanning electron microscopy (SEM) image, where the aggregated irregular structure at the micron level can be clearly seen, and the energy-dispersive X-ray spectroscopy (EDS) mapping displays that four elements including C, O, N and Br are dispersed on its surface (Fig. 1a). The powder X-ray diffraction (PXRD) pattern shows that the sample is in crystalline state(Fig. S3). In addition, the thermogravimetric analysis (TGA) reveals that **TPT-COOCH₃·Br** maintains the thermal stability up to 173 °C (Fig. S4).

3.2. Photoactivity and reversibility of TPT-COOCH₃·Br

In the solid-state UV-Vis absorption spectrum of **TPT-COOCH₃·Br**, besides a strong peak corresponding to the π-π transition at 264 nm (Fig. S5), a broad peak between 350 and 630 nm also appears. This broad peak vanishes when **TPT-COOCH₃·Br** is dissolved in solution, suggesting the occurrence of strong intermolecular charge transfer (CT) interaction in the solid state [33,34]. **TPT-COOCH₃·Br** in the solid state is extremely sensitive to ultraviolet light (365 nm), turning from yellow to orange within 15 s of light irradiation under air atmosphere. IR spectrum after irradiation is nearly identical with that of the original sample, excluding the possibility of photolysis (Fig. S6). It is noted that a new broad peak in the range of 650–865 nm emerges during this

photochromic process, accompanied by the gradual increase of absorption intensity with irradiation time (Fig. 1b). Moreover, unlike the original state, the photo-irradiated sample exhibits an ESR signal with the *g* value of 2.0039 after coloration (Fig. 1c), suggesting that the photochromism is a result of pyridinium radicals generated by photo-induced electron transfer (PET). The small shift towards higher binding-energy region can be observed in the core-level XPS spectra of O 1s and Br 3d after the irradiation, confirming that the O atoms in the ester group and free Br⁻ anions may serve as electron donors (details in Fig. S7). Furthermore, a change occurs in the N 1s core-level spectra (Fig. 1d), that is the peaks attributed to the triazine N atoms (399.4 eV) and positively charged N atoms (401.5 eV) move a little to the lower binding energy after coloration, and a new strong peak at 399.8 eV appears, which proves that the positively charged N atoms in **TPT-COOCH₃** moiety accept electrons from Br⁻ anion and ester O atom to give pyridinium radicals [35].

The weak ESR signal and low absorbance of the pyridinium radicals indicate that the efficiency of photoinduced electron transfer (PET) involving photocatalysts themselves is poor. Such a character should be conducive to the PET from alcohols to **TPT-COOCH₃** by reducing the competition. The orange sample fads to yellow and becomes ESR silent in a very short time upon exposure to darkness and air atmosphere (Figs. 1b and 1c). This observation indicates that this pyridinium radical
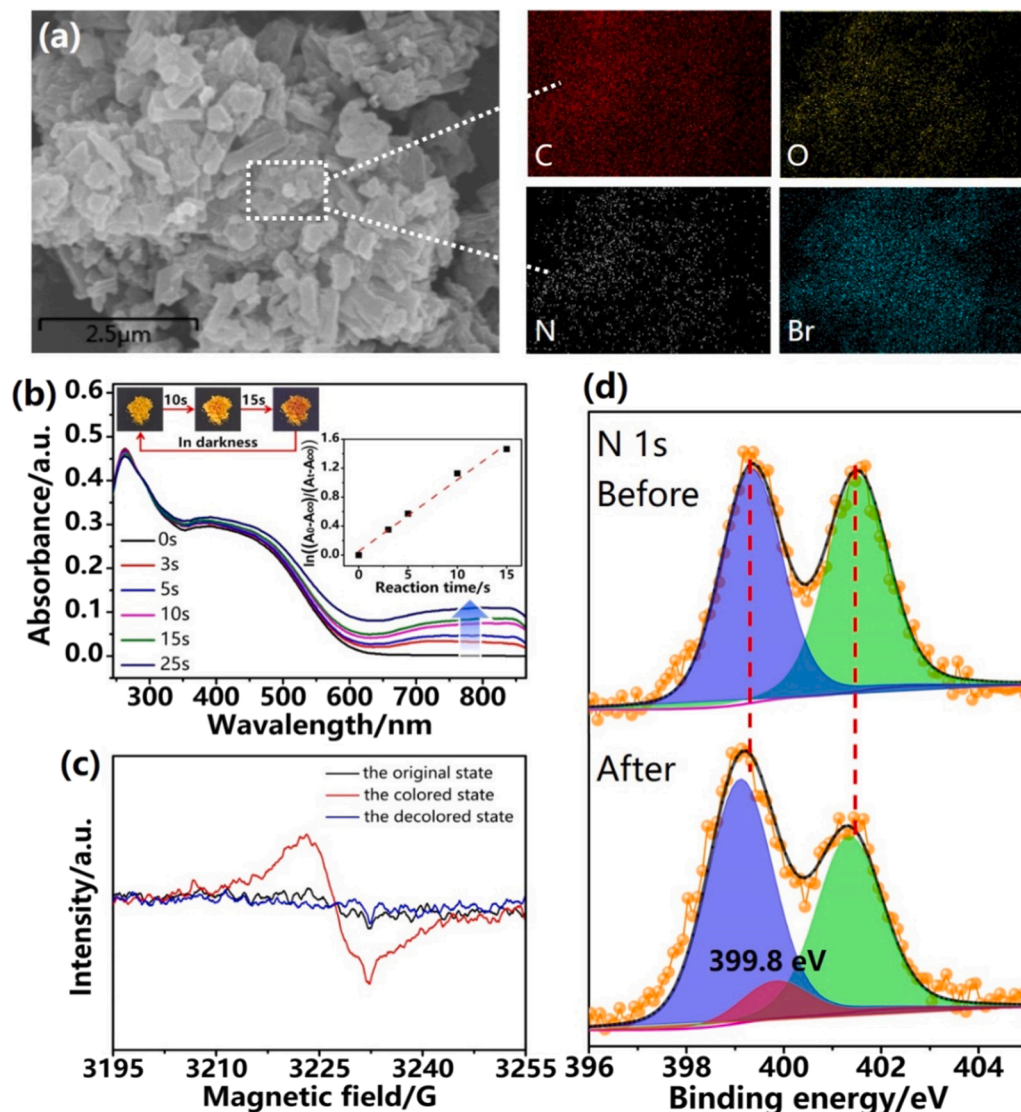

Fig. 1. (a) SEM image of **TPT-COOCH₃·Br** and the corresponding EDS mapping for element C (red), O (yellow), N (white) and Br (cyan). (b) UV-Vis diffuse reflectance absorption spectral changes of **TPT-COOCH₃·Br** under 365 nm light irradiation under air atmosphere. The insert shows time-dependent coloration and fading phenomena, as well as an approximate first-order kinetic plot for photochromism based on the absorbance at 773 nm. (c) Solid-state ESR spectra of **TPT-COOCH₃·Br** in original state (black line); colored state (red line); decolored state (blue line) under air atmosphere. (d) XPS core-level spectra of N 1s in **TPT-COOCH₃·Br** before and after 365 nm light irradiation.

•(**TPT-COOCH₃**) is quite oxygen-sensitive and can be quenched by molecular O_2 to revert to the initial **TPT-COOCH₃** cationic state with the simultaneous generation of •O_2^- radicals [36], demonstrating excellent redox reversibility and ability of **TPT-COOCH₃** to activate molecular oxygen and its potential in oxidation reaction as an electron-transfer photocatalyst.

3.3. Photocatalytic performance of TPT-COOCH₃·Br

TPT-COOCH₃·Br is slightly soluble in common solvents, can be completely dissolved in acetonitrile to give colorless solution below the concentration of 2.4×10^{-4} M as determined by a plot of absorbance versus concentration (details in Fig. S8). Therefore, a homogeneous catalytic reaction involving **TPT-COOCH₃·Br** for photoinduced aerobic oxidation of 4-methoxybenzyl alcohol (**1a**) to the corresponding carboxylic acid was explored in acetonitrile under mild conditions (details in Table 1). It is worth mentioning that the loading of catalyst (1 mol%) used in our system is smaller as compared to most of reported homogeneous systems (Table S1). Only trace amounts of acids were observed when the catalytic reaction proceeded without catalyst or in darkness, excluding the autoxidation of alcohols and indicating the necessity of light source. It was found that 365 nm light promoted the formation of 4-methoxybenzoic acid (**1b**) far more effectively than 395 nm light and white light within 90 min (Fig. S9), therefore the catalytic reaction was mainly carried out under 365 nm light irradiation. Furthermore, the output power of light source made an obvious effect on the catalytic effect, that is, the yield of acid product raised

gradually with increasing light intensity (Fig. S10). The investigation on catalyst loading revealed that the yield of carboxylic acid increased with an increase in catalyst loading, going up to 60% from 29% when the catalyst amount was varied in the range of 0.25–1.00 mol% (Fig. S11). By using the pure oxygen instead of air, the yield of the carboxylic acid was improved under the same irradiation time (Fig. S12). Nevertheless, from the perspective of sustainable development, the low-cost and safer air was still the best choice for this reaction. In addition, the conversion of alcohol to acid couldn't occur once choosing **TPT** or KBr as the catalyst instead of **TPT-COOCH₃·Br**, not only

revealing the crucial role of the pyridinium core, but also excluding the influence of bromide anion.
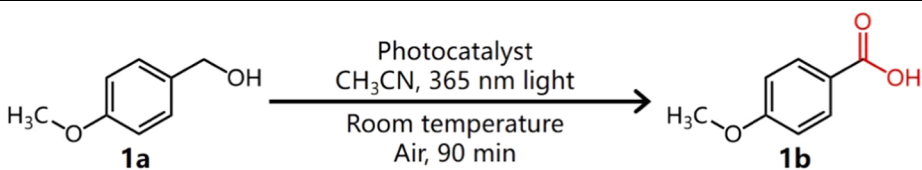
From time-dependent photocatalytic oxidation curves of **1a** (Fig. 2a), it was found that there were no acids but a large number of aldehydes emerging at the first 30 min, next the appearance of **1b** led to a reduced formation rate of aldehyde, even some of which began to decline in yield after 60 min. Although the alcohol has been completely absent at 90 min, the consumption of aldehyde and formation of acid continued to proceed until the end of the reaction. As the irradiation time extended to 180 min, the yield of acid reached nearly 93% finally with the formation of photolysis product anisole in 7% yield. The apparent quantum efficiency (AQE) for the oxidation of 4-methoxybenzyl alcohol by **TPT-COOCH₃·Br** at 365 nm is 3% [37]. This observation pointed out that the conversion process from alcohols to target acids over **TPT-COOCH₃·Br** consisted of two consecutive procedures: oxidation of the alcohol to form the intermediate aldehyde, and subsequent oxidation to produce carboxylic acid. The almost unchanged ^{1}H NMR spectra of **TPT-COOCH₃·Br** before and after the photocatalytic reaction demonstrated the high stability of the catalyst and its great potential for recycling in the selective oxidation of alcohols to acids (Fig. S13).

3.4. Photocatalytic mechanism investigation of TPT-COOCH₃·Br

The different oxidation performance of **TPT-COOCH₃·Br** in various gas environments (air, O_2 and N_2) indicates the key contribution of O_2 during the reaction process (Fig. S12). To clarify the active species generated in the photocatalytic system, a series of scavenger-quenching experiments were conducted under the optimized conditions for elucidating the reaction mechanism (Fig. 2b and Table S2). During this process, the irradiation time was set to 90 min for a convenient and consistent comparison. In the presence of **1a**, the potential reactive oxygen species (ROS), such as hydroxyl radical (•OH), singlet oxygen ($^1O_2$), superoxide anion radical (•O_2^-) were investigated by adding the corresponding scavengers tert-butyl alcohol (TBA), sodium azide (NaN₃), benzoquinone (BQ). Additionally, silver nitrate (AgNO₃) was also used for assessing the participation of electrons. Compared to the yield of acid in the absence of scavengers, the addition of TBA didn't

Table 1
Exploration and optimization for aerobic oxidation of 4-methoxybenzyl alcohol to carboxylic acid.[a]

Entry	Photocatalyst	Light source	1b[b] (%)
1	No catalyst	365 nm	trace
2	**TPT-COOCH₃·Br**	Darkness	trace
3	**TPT-COOCH₃·Br**	365 nm	60
4[c]	**TPT-COOCH₃·Br**	395 nm	5
5[d]	**TPT-COOCH₃·Br**	White light	trace
6[e]	**TPT-COOCH₃·Br**	365 nm	trace
7[f]	**TPT-COOCH₃·Br**	365 nm	trace
8[g]	**TPT-COOCH₃·Br**	365 nm	12
9[h]	**TPT-COOCH₃·Br**	365 nm	46
10	0.25 mol% **TPT-COOCH₃·Br**	365 nm	29
11	0.5 mol% **TPT-COOCH₃·Br**	365 nm	36
12	0.75 mol% **TPT-COOCH₃·Br**	365 nm	51
13[i]	**TPT-COOCH₃·Br**	365 nm	69
14[j]	**TPT**	365 nm	trace
15[k]	KBr	365 nm	trace

[a]Standard reaction conditions: 4-methoxybenzyl alcohol (0.1 mmol) and photocatalyst (1 mol%) in acetonitrile (5 mL) at room temperature and 1 atm air for 90 min under 365 nm light. Unless otherwise specified, the power of 365 nm LED light is 100% (light intensity: 298 mW cm^{-2}). [b]Yields of **1b** were derived from GC. [c]395 nm LED light (light intensity: 607 mW cm^{-2}). [d]White LED light (light intensity: 307 mW cm^{-2}). [e]The power of 365 nm light is 20%. [f]The power of 365 nm light is 40%. [g]The power of 365 nm light is 60%. [h]The power of 365 nm light is 80%. [i]In pure oxygen atmosphere. [j]**TPT** (1 mol%): 2,4,6-tri(4-pyridyl)-1,3,5-triazine. [k]KBr (1 mol%): potassium bromide.
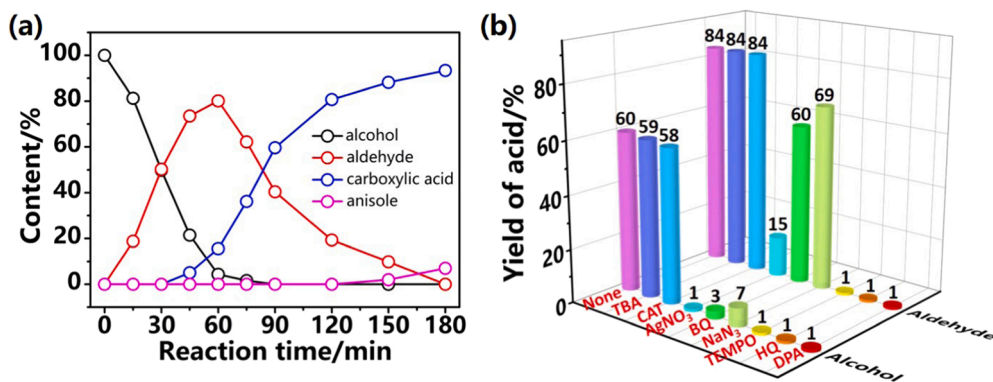
Fig. 2. (a) The change in the content of substrate and products during the oxidation of 4-methoxybenzyl alcohol by **TPT-COOCH₃·Br** within 180 min under the optimized conditions. (b) Inhibition impact of different scavengers on the acid yield using 4-methoxybenzyl alcohol or 4-methoxybenzaldehyde as substrate, respectively (reaction time: 90 min).

cause any change, while adding AgNO₃, BQ or NaN₃ had a considerable inhibition impact in the order of AgNO₃ > BQ > NaN₃. The study clearly indicates that besides electrons, this catalytic process also involves the participation of ${}^{\bullet}O_2^{-}$ and ${}^{1}O_2$. The direct evidence for the formation of ${}^{\bullet}O_2^{-}$ and ${}^{1}O_2$ was confirmed by ESR measurements. Four characteristic peaks for DMPO-${}^{\bullet}O_2^{-}$ spin adducts (1:2:2:1), or three characteristic peaks for TEMP-${}^{1}O_2$ spin adducts (1:1:1) could be observed respectively (Figs. 3a and 3b) after introducing spin-trapping agent 5,5-dimethyl-1-pyrroline *N*-oxide (DMPO) or 2,2,6,6,-tetramethylpiperidine (TEMP) into photocatalytic system for identifying ${}^{\bullet}O_2^{-}$ and ${}^{1}O_2$. Remarkably, there were no DMPO-${}^{\bullet}O_2^{-}$ spin adducts, but stronger TEMP-${}^{1}O_2$ spin adducts emerging in the absence of alcohols, suggesting that the electron transfer was low-efficient in the absence of alcohols, thus allowing the energy transfer from the excited state (**TPT-COOCH₃**)* to O₂ to generate ${}^{1}O_2$. Furthermore, both of those characteristic ESR signals disappeared by adding SOD or NaN₃, respectively. The fact that the yield of acid was seriously suppressed by radical scavengers, for example 2,2,6,6-tetra-methylpiperidine-*N*-oxyl (TEMPO), hydroquinone (HQ), and

diphenylamine (DPA), demonstrated that this oxidation reaction indeed proceeded in a radical pathway, where the oxygen-centered and carbon-centered radicals coexisted [38,39]. On the other hand, the direct oxidation of aldehydes also occurred with **TPT-COOCH₃·Br** (Fig. S14), which strongly verified our speculation about two consecutive procedures in selectively converting alcohols to acids. Amazingly, the inhibition impact of scavengers on the aldehyde oxidation was also observed as that on the alcohol oxidation mentioned above (Fig. 2b and Table S3, entries 1–10). Combined with the detected ESR signals associated to ${}^{\bullet}O_2^{-}$ and ${}^{1}O_2$ species in this aldehyde-acid transformation system (Fig. S15), these results reveal that the conversion from aldehydes into acids catalyzed by **TPT-COOCH₃·Br** also involves the participation of electron, ${}^{\bullet}O_2^{-}$ and ${}^{1}O_2$, the oxygen-centered

and carbon-centered radicals. In addition, the potential oxidant H₂O₂ was detected by the UV-Vis absorption spectroscopic measurement (Fig. S16), while it had almost no effect on the yield of acid as proved by adding the scavenger catalase (CAT).

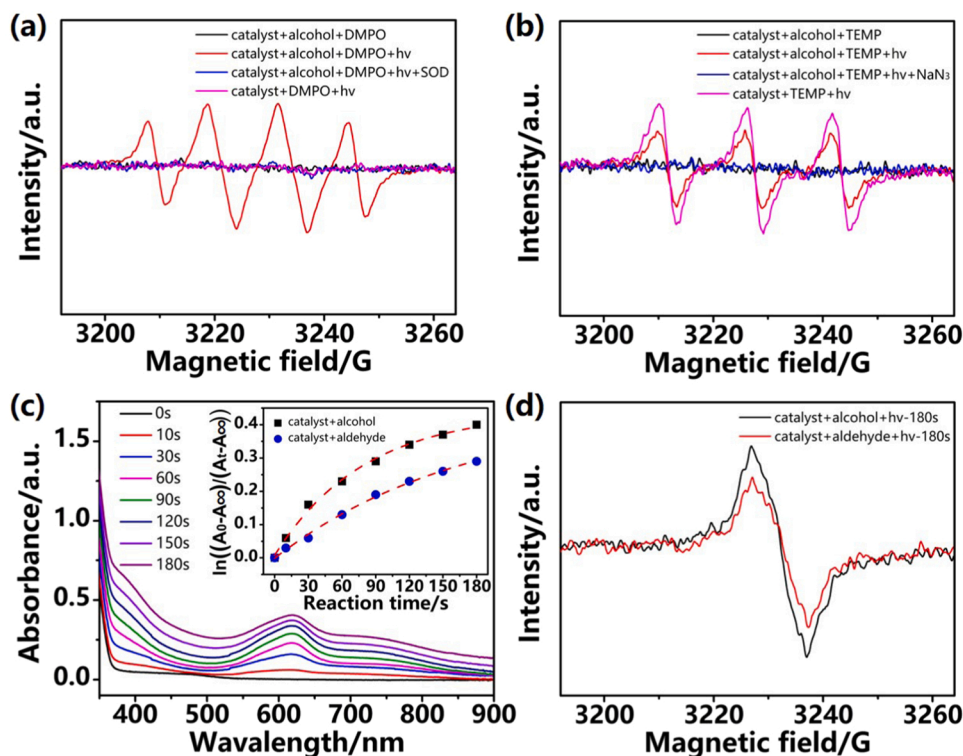It was also found that the inhibition impact of BQ and NaN₃ was not

Fig. 3. (a) DMPO-${}^{\bullet}O_2^{-}$ ESR spectra of **TPT-COOCH₃·Br** with DMPO in the presence of alcohol in darkness (black line), upon 365 nm light before (red line) and after (blue line) adding SOD, or in the absence of alcohol upon 365 nm light (pink line) under air atmosphere. (b) TEMP-${}^{1}O_2$ ESR spectra of **TPT-COOCH₃·Br** with TEMP in the presence of alcohol in darkness (black line), upon 365 nm light before (red line) and after (blue line) adding NaN₃, or in the absence of alcohol upon 365 nm light (pink line) under air atmosphere. (c) UV-Vis absorption spectral changes of **TPT-COOCH₃·Br** with alcohol within 180 s of irradiation by 365 nm light in acetonitrile under nitrogen atmosphere. The insert shows the comparison of second-order reaction kinetic curves based on the absorbance at 619 nm in the presence of alcohol or aldehyde. (d) ESR spectra of **TPT-COOCH₃·Br** in the presence of alcohol (black line) or aldehyde (red line) after 180 s of irradiation by 365 nm light in acetonitrile.

obvious enough for the direct oxidation of aldehydes to acids by using **TPT-COOCH₃·Br**. To explain this, a reasonable hypothesis was proposed: besides the catalytic transformation process, parts of aldehydes might be autoxidized non-catalytically to acids [40,41]. In the control experiment, the transformation in the absence of catalyst really happened, while the yield of acid was lower than that with catalyst (Fig. S14). The acid yield was almost unchanged after the addition of BQ or NaN₃, whereas it declined dramatically when the air was evacuated and replaced by nitrogen (Table S3, entries 11–14), exhibiting that O₂ is necessary for the autoxidation of aldehydes. Therefore, the oxidation of aldehydes into acids in current photoreaction system is a combination of the catalytic oxidation employing $^{\bullet}O_2^-$ and $^1O_2$ and the autoxidation where O₂ is a key factor.

Besides the participation in autoxidation, O₂ is also important for the catalytic oxidation of whether alcohols or aldehydes. No matter the conversion of alcohols or aldehydes is greatly inhibited under the nitrogen atmosphere. We infer that the important role of O₂ in our photocatalytic reaction involves two aspects: (1) forming the main ROS, such as $^{\bullet}O_2^-$ and $^1O_2$, through the electron transfer or energy transfer; (2) achieving the cycle of catalyst via oxidizing $^{\bullet}$(**TPT-COOCH₃**) radicals back to its initial state. The second conclusion was confirmed by the time-dependent coloration and fading phenomena of **TPT-COOCH₃·Br** in the presence of alcohols or aldehydes. Under the continuous irradiation with 365 nm light, the colorless mixture in acetonitrile under nitrogen atmosphere gradually turned green within 180 s (Fig. S17a). Meanwhile, both showed the new characteristic absorption peak at 619 nm that increased with the irradiation time (Figs. 3c and S17b) and strong ESR signal (g = 2.0012 or 2.0010) (Fig. 3d), similar to those of pyridinium radicals. This outcome was indicative of the occurrence of photoinduced electron transfer (PET) from alcohols or aldehydes to the positively charged pyridinium moiety, which was further confirmed by Stern-Volmer fluorescence quenching experiments (Fig. S18) [42]. Although the bromide anion and ester O atom probably served as the donor for PET, the poor photochromic performance for **TPT-COOCH₃·Br** in acetonitrile under nitrogen atmosphere in the absence of any substrate with extended irradiation time of 60 min, as shown by the weak UV–vis absorption and ESR spectral changes (Fig. S19), not only showed that the main electron donor was still alcohols or aldehydes, but also ruled out the influence of charge-balancing bromide anion and ester O atom on the catalytic efficiency from the competitive effect. By comparing the second-order reaction kinetic curves of photochromism (The inset in Fig. 3c) as well as the ESR signals of pyridinium radical (Fig. 3d) and $^{\bullet}O_2^-$ (Fig. S20) in the presence of an equal amount of

alcohol or aldehyde under the identical light irradiation, it was observed that alcohol was a stronger donor than aldehyde in the process of electron transfer. The colored state of **TPT-COOCH₃·Br** in acetonitrile was extremely unstable once contacting with air, meaning that the pyridinium radical was effectively quenched by O₂, as proved by the disappearance of the long-wavelength absorption band (Fig. S21) and ESR signal (Fig. S22).

Combined with all of the experimental information, the reaction mechanism of **TPT-COOCH₃·Br** for the aerobic oxidation of alcohols into acids was proposed (Scheme 2). Firstly the catalytic oxidation of alcohols into aldehydes as well as the byproduct hydrogen peroxide under the irradiation of 365 nm light were achieved by $^{\bullet}O_2^-$ and $^1O_2$, obtained via the activation of O₂ in the electron transfer or energy transf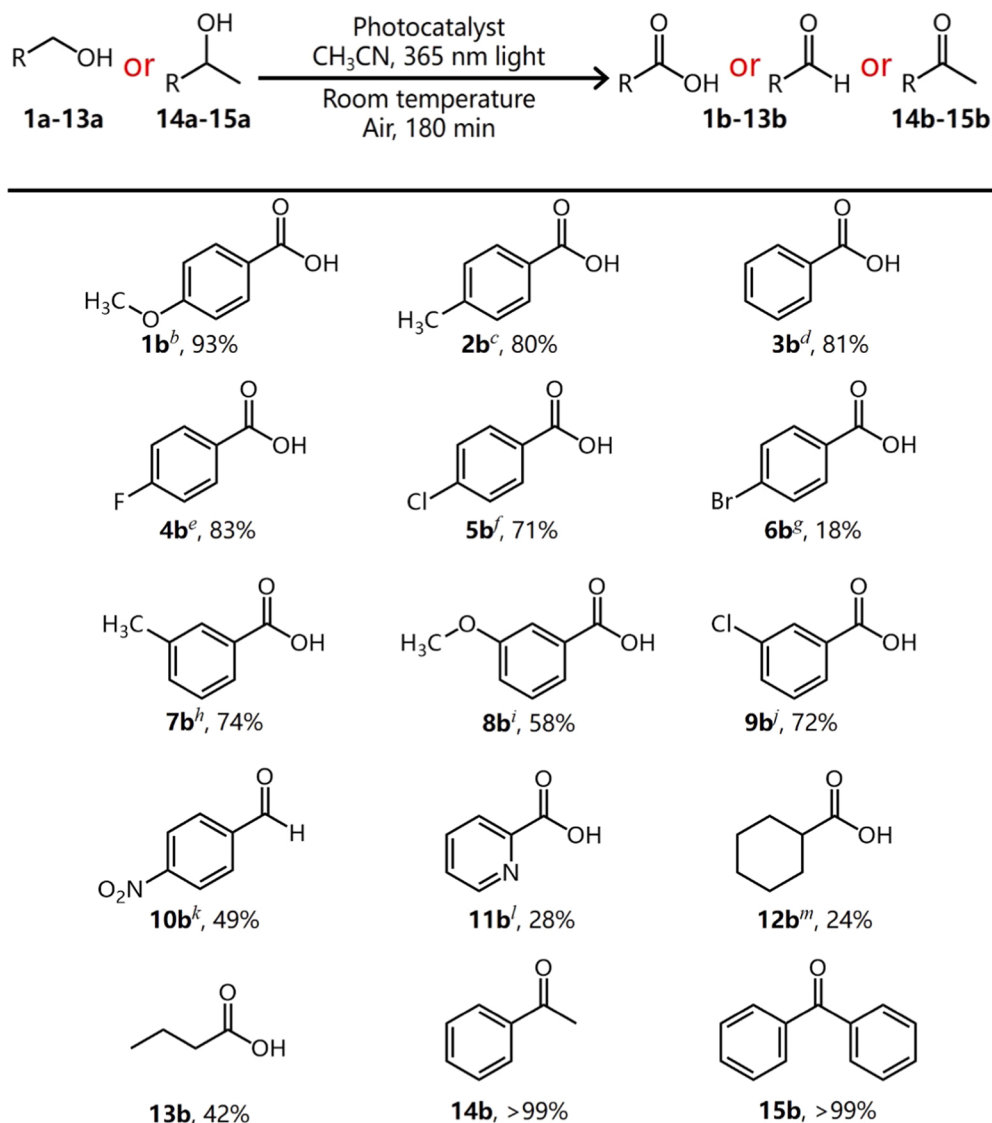er process [32]. Then the transformation of aldehydes into carboxylic acid could be divided into two sections. On one side, the electron transfer from aldehydes to **TPT-COOCH₃·Br** made the formation of carbon-centered radical (**A**). Next **A** could react with $^{\bullet}O_2^-$ to form the hydroperoxide (**D**) directly. On the other side, the autoxidation of aldehydes by means of photolysis produced another carbon-centered radical (**B**) which would transfer into the peroxy radical (**C**) with the aid of $^1O_2$ and O₂. Subsequently, the combination between **C** and aldehydes initiated a peroxidation chain reaction [43] involving the appearance of **D** by forming the O—H bond and regeneration of **B** through breaking the benzylic C—H bond. At last, the product acids were generated in the Baeyer-Villiger reaction [44] by using **D** with aldehydes.

3.5. Photocatalytic scope of TPT-COOCH₃·Br

Remarkably, the catalyst **TPT-COOCH₃·Br** owns the ability to promote the transformation of most common aromatic primary alcohols into the corresponding carboxylic acids in 58–93% yields within 180 min (Table 2, entries 1b–9b). Even though there are varying degrees of photolysis phenomena (details in Table 2), the influence of the electronic effect and position of functional group on the acid yield is also reflected roughly: the yield of acid corresponding to the alcohol with electron-donating group at *para* position is higher than that with electron-withdrawing group at the same position as well as the same group at *meta* position [45]. So the existence of stronger electron-withdrawing nitro group leads to the result that no acid but 49% of 4-nitrobenzaldehyde with > 99% selectivity is formed even prolonging the irradiation time to 360 min (Table 2, entry 10b). Substrates including heteroaromatic, alicyclic, and aliphatic primary
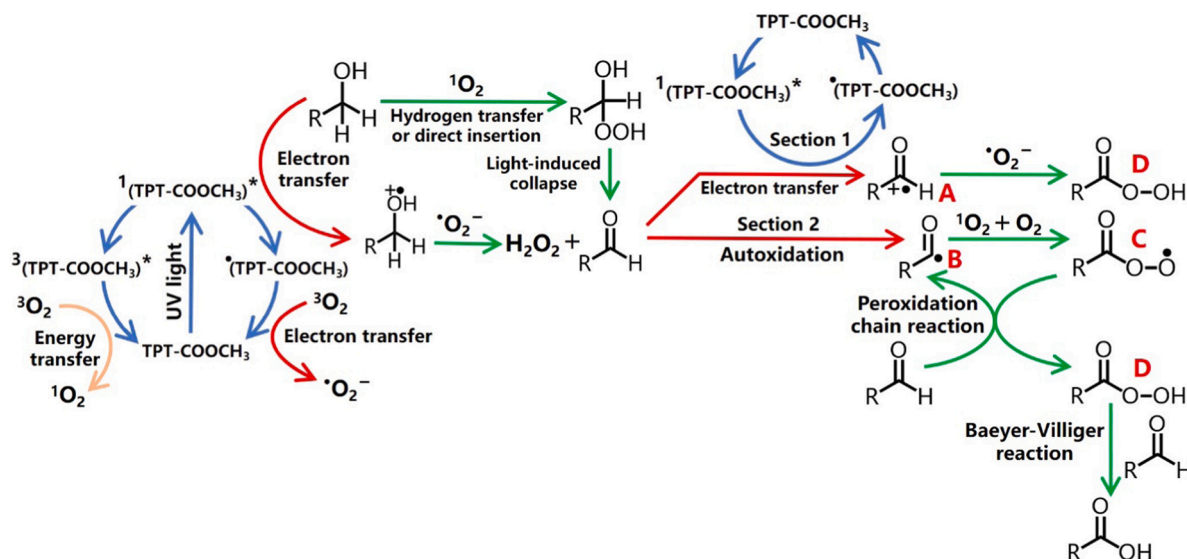
Scheme 2. Plausible reaction mechanism for light-induced aerobic oxidation of alcohols to carboxylic acids by using TPT-COOCH₃·Br.

Table 2

Yields for oxidation of primary and secondary alcohols to carbonyl compounds catalyzed by TPT-COOCH₃·Br.[a]

1b[b], 93%   **2b**[c], 80%   **3b**[d], 81%

4b[e], 83%   **5b**[f], 71%   **6b**[g], 18%

7b[h], 74%   **8b**[i], 58%   **9b**[j], 72%

10b[k], 49%   **11b**[l], 28%   **12b**[m], 24%

13b, 42%   **14b**, >99%   **15b**, >99%

[a]Standard reaction conditions: alcohol (0.1 mmol) and photocatalyst (1 mol%) in acetonitrile (5 mL) at room temperature and 1 atm air for 180 min under 365 nm light with 100% power (light intensity: 298 mW cm⁻²). Yield for oxidation product was derived from GC. It was noted that during the oxidation of alcohols, different photolysis products were generated as follows: [b]Yield of anisole is 7%. [c]Yield of toluene is 13%. [d]Yield of benzene is 11%. [e]Yield of fluorobenzene is 12%. [f]Yield of chlorobenzene is 14%. [g]Yield of bromobenzene is 10%. [h]Yield of toluene is 15%. [i]Yield of anisole is 20%. [j]Yield of chlorobenzene is 17%. [k]No acid but 49% of 4-nitro-benzaldehyde with > 99% selectivity was formed even after irradiation for 360 min [l]Yield of pyridine is 35%. [m]Yield of cyclohexane is 9%.

alcohols are also tolerated in the catalytic reaction (Table 2, entries 11b–13b). Significantly, the turnover frequency (TOF) obtained by the oxidation of 1-butanol into 1-butyric acid for **TPT-COOCH₃·Br** is comparable to or better than that for most homogeneous catalysts (Table S4). Once utilizing 1-phenylethanol or diphenylmethanol as the substrate, they are fully converted into ketones in 100% selectivity without any photolysis products (Table 2, entries 14b and 15b), showing the better efficiency of **TPT-COOCH₃·Br** from the aspect of yield than other reported photocatalysts in the oxidation of aromatic secondary alcohols (Table S5). Taken together, **TPT-COOCH₃·Br** exhibits the excellent photocatalytic activity in selectively converting alcohols with a broad substrate scope, especially aromatic alcohols.

3.6. Recycling of homogeneous system involving TPT-COOCH₃·Br

It was interesting to note that different amounts of white

precipitation appeared under the optimized conditions if extending the irradiation time and increasing the dosage of substrate to 20 times (2.0 mmol) simultaneously for various substrates (Fig. 4a). The precipitation is easy to be separated from the catalytic reaction mixture by a simple method of filtration, giving the white

powder of respective product acid confirmed by comparing IR spectra (Fig. S23). Although the acids corresponding to various substrates have been formed, the precipitation phenomena are apt to occur in the reaction systems forming acids with low solubility in acetonitrile (Fig. S24). That means that the poorer solubility the product owns, the higher yield the precipitation gives. It is worth noting that after the reaction is completed, different color changes can be seen in the mixture containing various substrates, however how to explain these phenomena is still in research. Moreover, as demonstrated by 4-chlorobenzyl alcohol which is easy to give the most amount of precipitation, the filtrate including the catalyst can be reused at least five times with high catalytic
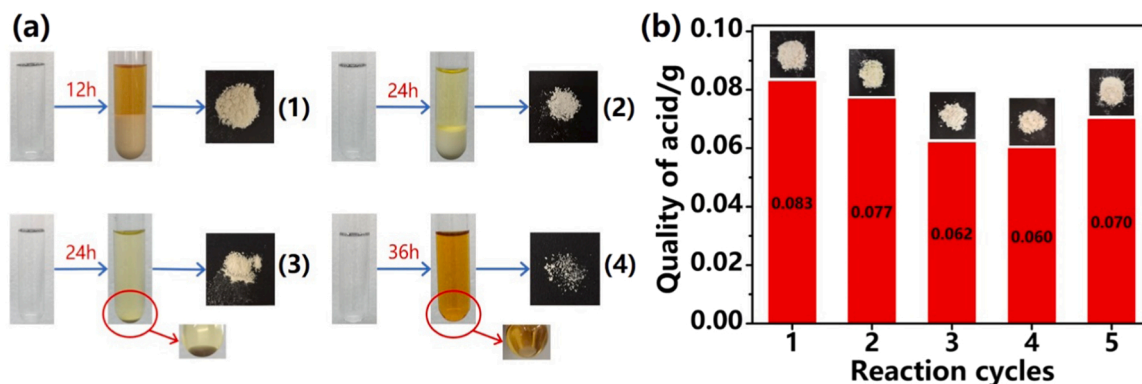
Fig. 4. (a) Precipitation phenomena of the products in catalytic reaction systems in the presence of 4-chlorobenzyl alcohol after light irradiation for 12 h (1), 4-methoxybenzyl alcohol for 24 h (2), 4-methylbenzyl alcohol for 24 h (3), 3-chlorobenzyl alcohol for 36 h (4). The yield of the precipitation decreases in the order of (1) > (2) > (3) > (4). (b) Quality of the acid precipitate within five catalytic reaction cycles in a case of 4-chlorobenzyl alcohol.

activity (Fig. 4b) by the repeated filtration to remove the acid (Fig. S25).

It is well known that the disadvantage involving the difficult separation of catalysts in the homogeneous catalytic system usually causes waste generation and an increase in the overall cost of the reaction systems. Thinking from the opposite perspectives, a simple isolation of the product by precipitation should be an efficient alternative to solve this problem. The high-performance and low loading of **TPT-COOCH₃·Br** promote the generation of abundant products, which are easily separated out from the system and removed by filtration to complete the recycling of homogeneous catalysts in the aerobic oxidation of alcohols to carboxylic acids. By comparison to those catalysts with similar strategies (Table S6) [23,24,46,47], **TPT-COOCH₃·Br** is the first reusable homogeneous electron-transfer catalyst for obtaining the product of carboxylic acid directly and efficiently, avoiding the use of corrosive base and complicated acidizing operation and rendering this photocatalytic system with great application potential in the future industrial production.

4. Conclusions

In summary, we have successfully developed an efficient and green protocol for the aerobic oxidation of alcohols into the corresponding acids by air based on pyridinium-based catalyst without the assistance of any metals and additives, which is also the first time that such a photocatalytic system has been applied in the synthesis of carboxylic acids from alcohols. The photocatalytic oxidation of alcohols to aldehydes, photocatalytic oxidation and autoxidation of aldehydes to acids are found to be involved in this reaction system. The scavenger-quenching experiments and ESR measurements demonstrate the generation of active oxygen species •O₂⁻ and ¹O₂ mediated by **TPT-COOCH₃·Br** via electron transfer and energy transfer, and their cooperative action during the catalytic oxidation process. Moreover, this catalyst has an excellent ability in promoting the conversion of abundant substrates by prolonging irradiation time. The product of carboxylic acid is precipitated from acetonitrile and then filtered out directly to achieve the reuse of the homogeneous system including **TPT-COOCH₃·Br**. The present work enriches the type of photocatalyst in selectively converting alcohols to acids, and more importantly, offers a practical and sustainable way to optimize the application performance of homogeneous catalysts.

Supporting Information

The following files are available free of charge: experimental procedure; additional characteristic figures and tables (Figs. S1–S25, Tables S1–S6) and gas chromatography details.

Author Contributions

The manuscript was written through contributions of all authors. All authors have given approval to the final version of the manuscript.

CRediT authorship contribution statement

Jing-Wang Cui: Conceptualization, Validation, Investigation, Writing – original draft, Writing – review & editing. **Shuai Ma:** Methodology. **Cai-Hui Rao:** Resources. **Meng-Ze Jia:** Formal analysis. **Xin-Rong Yao:** Software. **Jie Zhang:** Conceptualization, Data curation, Writing – review & editing, Supervision, Funding acquisition.

Declaration of Competing Interest

The authors declare that they have no known competing financial interests or personal relationships that could have appeared to influence the work reported in this paper.

Acknowledgment

Appendix A. Supporting information

Supplementary data associated with this article can be found in the online version at doi:10.1016/j.apcatb.2021.121028.

References

[1] E. Balaraman, E. Khaskin, G. Leitus, D. Milstein, Catalytic transformation of alcohols to carboxylic acid salts and H2 using water as the oxygen atom source, Nat. Chem. 5 (2013) 122–125.
[2] Y.T. Liao, V.C. Nguyen, N. Ishiguro, A.P. Young, C.K. Tsung, K.C.W. Wu, Engineering a homogeneous alloy-oxide interface derived from metal-organic frameworks for selective oxidation of 5-hydroxymethylfurfural to 2,5-furandicarboxylic acid, Appl. Catal. B 270 (2020), 118805.
[3] X. Jiang, J. Zhang, S. Ma, Iron catalysis for room-temperature aerobic oxidation of alcohols to carboxylic acids, J. Am. Chem. Soc. 138 (2016) 8344–8347.
[4] J. Ding, W. Xu, H. Wan, D. Yuan, C. Chen, L. Wang, G. Guan, W.L. Dai, Nitrogen vacancy engineered graphitic C3N4-based polymers for photocatalytic oxidation of aromatic alcohols to aldehydes, Appl. Catal. B 221 (2018) 626–634.
[5] P. Chandra, T. Ghosh, N. Choudhary, A. Mohammad, S.M. Mobin, Recent advancement in oxidation or acceptorless dehydrogenation of alcohols to valorised products using manganese based catalysts, Coord. Chem. Rev. 411 (2020), 213241.
[6] C. Zhu, J. Liu, M.B. Li, J.E. Backvall, Palladium-catalyzed oxidative dehydrogenative carbonylation reactions using carbon monoxide and mechanistic overviews, Chem. Soc. Rev. 49 (2020) 341–353.
[7] A. Sarbajna, I. Dutta, P. Daw, S. Dinda, S.M.W. Rahaman, A. Sarkar, J.K. Bera, Catalytic conversion of alcohols to carboxylic acid salts and hydrogen with alkaline water, ACS Catal. 7 (2017) 2786–2790.

[8] K. Fujita, R. Tamura, Y. Tanaka, M. Yoshida, M. Onoda, R. Yamaguchi, Dehydrogenative oxidation of alcohols in aqueous media catalyzed by a water-soluble dicationic iridium complex bearing a functional N-heterocyclic carbene ligand without using base, ACS Catal. 7 (2017) 7226–7230.

[9] V. Cherepakhin, T.J. Williams, Iridium catalysts for acceptorless dehydrogenation of alcohols to carboxylic acids: scope and mechanism, ACS Catal. 8 (2018) 3754–3763.

[10] F. Monda, R. Madsen, Zinc oxide-catalyzed dehydrogenation of primary alcohols into carboxylic acids, Chem. Eur. J. 24 (2018) 17832–17837.

[11] D. Gong, B. Hu, D. Chen, Bidentate Ru(II)-NC complexes as catalysts for the dehydrogenative reaction from primary alcohols to carboxylic acids, Dalton Trans. 48 (2019) 8826–8834.

[12] D.R. Pradhan, S. Pattanaik, J. Kishore, C. Gunanathan, Cobalt-catalyzed acceptorless dehydrogenation of alcohols to carboxylate salts and hydrogen, Org. Lett. 22 (2020) 1852–1857.

[13] L. Clarizia, D. Russo, I. Di Somma, R. Marotta, R. Andreozzi, Homogeneous photo-Fenton processes at near neutral pH: a review, Appl. Catal., B 209 (2017) 358–371.

[14] S. Fukuzumi, K. Ohkubo, Organic synthetic transformations using organic dyes as photoredox catalysts, Org. Biomol. Chem. 12 (2014) 6059–6071.

[15] Y. Zhang, W. Schilling, D. Riemer, S. Das, Metal-free photocatalysts for the oxidation of non-activated alcohols and the oxygenation of tertiary amines performed in air or oxygen, Nat. Protoc. 15 (2020) 822–839.

[16] W. Schilling, D. Riemer, Y. Zhang, N. Hatami, S. Das, Metal-free catalyst for visible-light-induced oxidation of unactivated alcohols using air/oxygen as an oxidant, ACS Catal. 8 (2018) 5425–5430.

[17] N.F. Nikitas, D.I. Tzaras, I. Triandafillidi, C.G. Kokotos, Photochemical oxidation of benzylic primary and secondary alcohols utilizing air as the oxidant, Green. Chem. 22 (2020) 471–477.

[18] X. Shi, S. Liu, C. Duanmu, M. Shang, M. Qiu, C. Shen, Y. Yang, Y. Su, Visible-light photooxidation of benzene to phenol in continuous-flow microreactors, Chem. Eng. J. 420 (2021) 129976.

[19] Q. Xia, Z. Shi, J. Yuan, Q. Bian, Y. Xu, B. Liu, Y. Huang, X. Yang, H. Xu, Visible-light-enabled selective oxidation of primary alcohols through hydrogen-atom transfer and its application in the synthesis of quinazolinones, Asian J. Org. Chem. 8 (2019) 1933–1941.

[20] Q. Li, F.T. Li, Recent advances in molecular oxygen activation via photocatalysis and its application in oxidation reactions, Chem. Eng. J. 421 (2021) 129915.

[21] Z. Yang, X. Xia, W. Yang, L. Wang, Y. Liu, Photothermal effect and continuous hot electrons injection synergistically induced enhanced molecular oxygen activation for efficient selective oxidation of benzyl alcohol over plasmonic $W_{18}O_{49}/ZnIn_2S_4$ photocatalyst, Appl. Catal. B 299 (2021), 120675.

[22] V.S. Shende, V.B. Saptal, B.M. Bhanage, Recent advances utilized in the recycling of homogeneous catalysis, Chem. Rec. 19 (2019) 2022–2043.

[23] C. Santilli, I.S. Makarov, P. Fristrup, R. Madsen, Dehydrogenative synthesis of carboxylic acids from primary alcohols and hydroxide catalyzed by a ruthenium N-heterocyclic carbene complex, J. Org. Chem. 81 (2016) 9931–9938.

[24] H.M. Liu, L. Jian, C. Li, C.C. Zhang, H.Y. Fu, X.L. Zheng, H. Chen, R.X. Li, Dehydrogenation of alcohols to carboxylic acid catalyzed by in situ-generated facial ruthenium-CPP complex, J. Org. Chem. 84 (2019) 9151–9160.

[25] J.K. Sun, X.D. Yang, G.Y. Yang, J. Zhang, Bipyridinium derivative-based coordination polymers: from synthesis to materials applications, Coord. Chem. Rev. 378 (2019) 533–560.

[26] L.X. Cai, S.C. Li, D.N. Yan, L.P. Zhou, F. Guo, Q.F. Sun, Water-soluble redox-active cage hosting polyoxometalates for selective desulfurization catalysis, J. Am. Chem. Soc. 140 (2018) 4869–4876.

[27] Y.R. Huang, X.L. Lin, B. Chen, H.D. Zheng, Z.R. Chen, H.H. Li, S.T. Zheng, Thermal-responsive polyoxometalate-metalloviologen hybrid: reversible intermolecular three-component reaction and temperature-regulated resistive switching behaviors, Angew. Chem. Int. Ed. 60 (2021) 16911–16916.

[28] Y. Amao, N. Shuto, H. Iwakuni, Ethanol synthesis based on the photoredox system consisting of photosensitizer and dehydrogenases, Appl. Catal. B 180 (2016) 403–407.

[29] Y. Zhou, F. Yu, J. Su, M. Kurmoo, J.L. Zuo, Tuning electrical- and photo-conductivity by cation exchange within a redox-active tetrathiafulvalene-based metal–organic framework, Angew. Chem. Int. Ed. 59 (2020) 18763–18767.

[30] Y. Zhao, M. Shalom, M. Antonietti, Visible light-driven graphitic carbon nitride (g-C_3N_4) photocatalyzed ketalization reaction in methanol with methylviologen as efficient electron mediator, J. Catal. B 207 (2017) 311–315.

[31] H. Ji, K. Naveen, W. Lee, T.S. Kim, D. Kim, D.H. Cho, Pyridinium-functionalized ionic metal-organic frameworks designed as bifunctional catalysts for CO_2 fixation into cyclic carbonates, ACS Appl. Mater. Interfaces 12 (2020) 24868–24876.

[32] S. Ma, J.W. Cui, C.H. Rao, M.Z. Jia, Y.R. Chen, J. Zhang, Boosting activity of molecular oxygen by pyridinium-based photocatalysts for metal-free alcohol oxidation, Green Chem. 23 (2021) 1337–1343.

[33] C. Chen, X.H. Jin, X.J. Zhou, L.X. Cai, Y.J. Zhang, J. Zhang, Photo-facilitated aggregation and correlated color temperature adjustment of single component organic solid state white-light emitting materials, J. Mater. Chem. C 3 (2015) 4563–4569.

[34] Y. Orimoto, K. Ishimoto, Y. Aoki, Role of pyridinium groups and iodide ions in photoelectrochromism in viologen-based ion-pair charge-transfer complexes: molecular orbital analysis, J. Phys. Chem. C 122 (2018) 4546–4556.

[35] M.S. Wang, C. Yang, G.E. Wang, G. Xu, X.Y. Lv, Z.N. Xu, R.G. Lin, L.Z. Cai, G. C. Guo, A room-temperature X-ray-induced photochromic material for X-ray detection, Angew. Chem. 51 (2012) 3432–3435.

[36] P.M.S. Monk, The Viologens: Physicochemical Properties, Synthesis and Applications of the Salts of 4,4′-Bipyridine, Wiley, Chichester, 1998.

[37] Y. Dai, P. Ren, Y. Li, D. Lv, Y. Shen, Y. Li, H. Niemantsverdriet, F. Besenbacher, H. Xiang, W. Hao, N. Lock, X. Wen, J.P. Lewis, R. Su, Solid base $Bi_{24}O_{31}Br_{10}(OH)_{\delta}$ with active lattice oxygen for efficient photo-oxidation of primary alcohols to aldehydes, Angew. Chem. Int. Ed. 58 (2019) 6265–6270.

[38] E. Rucinska, P.J. Miedziak, S. Pattisson, G.L. Brett, S. Iqbal, D.J. Morgan, M. Sankar, G.J. Hutchings, Cinnamyl alcohol oxidation using supported bimetallic Au-Pd nanoparticles: an investigation of autoxidation and catalysis, Catal. Sci. Technol. 8 (2018) 2987–2997.

[39] W. Zhong, M. Liu, J. Dai, J. Yang, L. Mao, D. Yin, Synergistic hollow CoMo oxide dual catalysis for tandem oxygen transfer: preferred aerobic epoxidation of cyclohexene to 1,2-epoxycyclohexane, Appl. Catal. B 225 (2018) 180–196.

[40] S. Mostrou, A. Nagl, M. Ranocchiari, K. Fottinger, J.A. van Bokhoven, The catalytic and radical mechanism for ethanol oxidation to acetic acid, Chem. Commun. 55 (2019) 11833–11836.

[41] M.J. Pavan, H. Fridman, G. Segalovich, A.I. Shames, N. Gabriel Lemcoff, T. Mokari, Photoxidation of benzyl alcohol with heterogeneous photocatalysts in the UV range: the complex interplay with the autoxidative reaction, ChemCatChem 10 (2018) 2541–2545.

[42] D.M. Arias-Rotondo, J.K. McCusker, The photophysics of photoredox catalysis: a roadmap for catalyst design, Chem. Soc. Rev. 45 (2016) 5803–5820.

[43] K.C. Hwang, A. Sagadevan, P. Kundu, The sustainable room temperature conversion of *p*-xylene to terephthalic acid using ozone and UV irradiation, Green Chem. 21 (2019) 6082–6088.

[44] G.J. ten Brink, I.W.C.E. Arends, R.A. Sheldon, The Baeyer-Villiger reaction: new developments toward greener procedures, Chem. Rev. 104 (2004) 4105–4123.

[45] I. Krivtsov, M. Ilkaeva, E.I. García-López, G. Marcì, L. Palmisano, E. Bartashevich, K. Matveeva, E. Grigorieva, E. Díaz, S. Ordóñez, Effect of substituents on photocatalytic partial oxidation of aromatic alcohols assisted by polymeric C_3N_4 photocatalysts, ChemCatChem 11 (2019) 2713–2724.

[46] E.W. Dahl, J. Louis-Goff, N.K. Szymczak, Second sphere ligand modifications enable a recyclable catalyst for oxidant-free alcohol oxidation to carboxylates, Chem. Commun. 53 (2017) 2287–2289.

[47] X. Wang, C. Wang, Y. Liu, J. Xiao, Acceptorless dehydrogenation and aerobic oxidation of alcohols with a reusable binuclear rhodium(II) catalyst in water, Green Chem. 18 (2016) 4605–4610.